



Xu Ke (Orcid ID: 0000-0002-6791-6393)

## Gravity-Induced Bubble Ripening in Porous Media and Its Impact on Capillary Trapping Stability

Ke Xu<sup>1</sup>, Yashar Mehmani<sup>2</sup>, Luoran Shang<sup>3</sup>, Qingrong Xiong<sup>4</sup>

<sup>1</sup> Department of Civil and Environmental Engineering, Massachusetts Institute of Technology, Cambridge, Massachusetts 02139, United States

<sup>2</sup> Department of Energy Resource Engineering, Stanford University, Stanford, California 94305, United States

<sup>3</sup> John A. Paulson School of Engineering and Applied Sciences, Harvard University, Cambridge, Massachusetts 02138, United States

<sup>4</sup> School of Mechanical, Aerospace & Civil Engineering, University of Manchester, M1 3BU, UK

Corresponding authors: Ke Xu, [xukethu@mit.edu](mailto:xukethu@mit.edu), and Yashar Mehmani [ymehmani@stanford.edu](mailto:ymehmani@stanford.edu)

### Key Points:

- Capillary trapping, although known to be hydrodynamically stable, may be thermodynamically unstable due to gravity induced Ostwald ripening
- Gravity modifies Ostwald ripening of trapped CO<sub>2</sub> bubbles, potentially leading to the formation of a gas cap and subsequent leakage risk
- A pore-scale model is upscaled to obtain a one-dimensional continuum model. Strategies for suppressing gravity-induced ripening are proposed

This article has been accepted for publication and undergone full peer review but has not been through the copyediting, typesetting, pagination and proofreading process which may lead to differences between this version and the Version of Record. Please cite this article as doi: 10.1029/2019GL085175

## Abstract

Capillary or residual trapping is considered one of the safest geologic CO<sub>2</sub> storage mechanisms due to its hydrodynamic stability. We present a first study of the impact of gravity on Ostwald ripening in porous media and show it may render capillary trapping thermodynamically unstable. Gravity induces a vertical chemical potential gradient that leads to the upwards diffusion of CO<sub>2</sub>. Thus, bubbles at shallower depths grow at the expense of bubbles in deeper strata, leading to the formation of an overriding gas cap. We first develop a pore-scale model for two bubbles trapped within adjacent pores, and then upscale it to obtain a one-dimensional continuum model. We use the latter to predict the macroscopic evolution of a trapped bubble population. Factors controlling the ripening process are isolated to assist in selecting CO<sub>2</sub> storage sites. Gravity-induced ripening may also play a role in geologic fluid emplacement and migration over millions of years.

## Plain Language Summary

Capillary trapping is a mechanism that ensures that the CO<sub>2</sub> injected during geologic carbon sequestration remains stable and safe underground. However, the stability of sequestered CO<sub>2</sub> can be disrupted by another competing mechanism called Ostwald ripening. In Ostwald ripening, CO<sub>2</sub> is transported from smaller bubbles towards larger bubbles. This is undesirable since large bubbles may become remobilized and potentially leak towards the surface. In this study, we show that gravity plays a crucial role in modifying the behavior of Ostwald ripening. Specifically, gravity causes an upwards migration of CO<sub>2</sub> towards shallower depths, which over long periods of time can lead to the formation of a mobile gas cap at the risk of leakage. The models we develop herein reveal that it is possible to decelerate or even prevent CO<sub>2</sub> migration if we carefully select sequestration sites that have the right kind of geology and rock type.

## 1. Introduction

The long-term stability of trapped CO<sub>2</sub> is paramount in geological CO<sub>2</sub> sequestration. Within the first ~10<sup>4</sup> years after injection, the dominant CO<sub>2</sub> trapping mechanisms include: structural and stratigraphic trapping (as mobile gas caps), solubility trapping (dissolved into resident brine), and residual or capillary trapping (as bubbles in pores) (Benson et al. 2012, Benson and Cole 2008, Benson and Orr 2008). Solubility trapping is limited by the dissolution capacity of the in-situ brine. Structural and stratigraphic trapping is less favorable over long times, as the mobile gas cap could leak through pre-existing faults and fractures (Guo et al. 2014). By comparison, residual trapping offers higher storage capacity (bubbles need not dissolve) and is more stable due to strong capillary forces at the pore scale (Hagoort 1988, Huppert and Neufeld 2014, Pentland et al. 2011). If the above physical trapping mechanisms remain effective over very long time scales (> 10<sup>4</sup> years), mineral trapping would dominate and permanently transform CO<sub>2</sub> into carbonate minerals (Xu, Apps and Pruess 2004).

Maximizing capillary trapping has therefore been the subject of intensive study over the past decade (Gasda, Nordbotten and Celia 2011, Gasda, Nordbotten and Celia 2009, Hesse, Orr and Tchelep 2008, Ide, Jessen and Orr Jr 2007, Juanes et al. 2006). Some predictions have suggested that more than 95% of the undissolved CO<sub>2</sub> can be safely sequestered through capillary trapping 10,000 years after injection (Gasda et al. 2009). By optimizing injection operations, residual trapping can be maximized while simultaneously preventing the formation of a gas cap (Ide et al. 2007). For these reasons Huppert et al. (Huppert and Neufeld 2014) have claimed that “residual trapping of fluid within porous rock is one of the most effective methods for stably trapping CO<sub>2</sub> after injection”.

While it is known that capillary trapping is hydrodynamically stable, its thermodynamic stability has been the subject of investigation only recently (Xu, Bonnecaze and Balhoff 2017, de Chalendar, Garing and Benson 2018, Garing et al. 2017). In the absence of geometric

confinement, Ostwald ripening (Fu, Cueto-Felgueroso and Juanes 2016, Voorhees 1985, Voorhees 1992) is the mechanism that causes the diffusion of CO<sub>2</sub> from small bubbles towards large bubbles. The driving force is the capillary pressure difference between the bubbles [Fig. 1(a)-(c)]. At equilibrium, Ostwald ripening leads to the formation of a single large bubble that may become hydrodynamically unstable (Fu et al. 2016). In the presence of confinement, however, the behavior of Ostwald ripening is modulated such that stable bubble configurations, with uniform capillary pressure, can exist. This observation has been confirmed by recent pore-scale (Xu et al. 2017) and core-scale (Garing et al. 2017) experiments, and pore-scale modeling (de Chalendar et al. 2018). Confinement affects Ostwald ripening because it imposes a constraint between the volume of a bubble ( $V_{bubble}$ ) and its capillary pressure ( $P_c$ ). The specific relationship between  $V_{bubble}$  and  $P_c$  depends on pore geometry. Fig. 1(f) shows such a relationship for the pore in Fig. 1(d)-(e). Note that  $P_c$  is a non-monotonic function of  $V_{bubble}$ , contrary to the case without confinement.  $P_c$  incurs a minimum,  $P_{c,min}$ , at bubble volume  $V_{crit}$ . For  $V_{bubble} < V_{crit}$ , the bubble is sufficiently small and does not contact the pore walls. It is spherical in shape and behaves identical to an unconfined bubble. For  $V_{bubble} > V_{crit}$ , the bubble cannot form a stable sphere inside the pore and is therefore squeezed into the narrow crevices and throats adjacent to the pore. The result is that  $P_c$  increases with  $V_{bubble}$ . Similar non-monotonic  $P_c$  functions have been used to model fluid-fluid displacements (Thompson 2002).

While recent studies (de Chalendar et al. 2018, Garing et al. 2017, Xu et al. 2017) have provided valuable insight into the effect of Ostwald ripening on capillary trapping, the influence of gravity has thus far been ignored. Neglecting gravity is indeed a reasonable assumption when studying hydrodynamic stability of trapped bubble because capillary forces at the pore scale are much stronger than buoyancy forces in the subsurface (Perkins and Johnston 1963, Whitaker 1967). However, during Ostwald ripening, bubbles interact with each

other through molecular diffusion without the need to physically mobilize. Since gravity can alter the magnitude and direction of chemical potential gradients, its contribution can no longer be neglected over long time periods. In the following, we show that gravity can cause a vertical redistribution of trapped bubbles in the reservoir leading to the formation of an overlying gas cap, which may pose subsequent risks of CO<sub>2</sub> leakage towards the surface.

## 2. Gravity-Induced Ripening at the Pore Scale

### 2.1. Model Description

In this section, we consider gravity-induced Ostwald ripening at the pore scale and develop a simplified model that captures the salient aspects of the physics. Consider the idealized two-bubble system depicted in Fig. 2(a). Two identical non-wetting bubbles of initial volume  $V_0$  are trapped within two identical pores separated by a vertical distance  $L_t$ . The throat connecting them has a cross-sectional area  $A_t$  and is filled with brine, which is the wetting phase  $w$ . The CO<sub>2</sub> bubbles comprise the non-wetting phase  $b$ . The two phases are slightly miscible and can therefore form a binary mixture. We assume that such a mixture forms only in the brine phase and that the CO<sub>2</sub> bubbles remain pure. For simplicity, we also use  $w$  and  $b$  to denote the water and CO<sub>2</sub> components, respectively. We further assume that the binary mixture is ideal and that the fluids are incompressible and under isothermal conditions. We aim to develop a one-dimensional model for this two-bubble system (full details in Supplementary Materials).

The  $P_c - V_{bubble}$  relation for a confined bubble is strongly dependent of the specific pore and throat shapes. For simplicity, but without loss of generality, we consider a linearized  $P_c - V_{bubble}$  relation given by  $P_c = g(m_1 V_{bubble}^{-1/3} + m_2 V_{bubble})$ , where  $\gamma$  is surface tension,  $m_1 = 4(\pi/6)^{1/3}$ ,  $m_2 \propto R_0^{-4}$ , and  $R_0$  is the pore half-length as marked in Fig. 1(d). The first term represents the contribution to  $P_c$  when  $V_{bubble} < V_{crit}$  and the bubble is spherical in shape. The second term

captures the contribution when  $V_{bubble} > V_{crit}$  and the bubble is deformed by the pore walls;  $P_c \approx \gamma m_2 V_{bubble}$  in this regime. Fig. 1(f) shows a graph of  $P_c$  versus  $V_{bubble}$  for  $m_2 = 2R_0^{-4}$ , which is the value used hereafter.

Denote the density and molar volume of the  $w$  and  $b$  phases by  $\rho_w$ ,  $V_{mw}$ ,  $\rho_b$ , and  $V_{mb}$ . Since  $\text{CO}_2$  is buoyant in brine in most common cases, we only consider  $\Delta\rho = \rho_w - \rho_b > 0$ . We initialize the bubble volumes such that  $V_0 > V_{crit}$ . Specifically, we set  $V_0 = 1.2R_0^3$ . We do not consider bubbles with  $V_0 < V_{crit}$ , because they are thermodynamically unstable (similar to unconfined bubble ripening) and thus uncommon after long time scales. We denote the pressure of the brine phase  $w$  with  $P$  and assume that it follows a steady-state hydrostatic profile.

We take the positive  $z$ -axis to coincide with the upward direction and place  $z = 0$  at the throat entrance connected to the bottom bubble. We choose a reference pressure  $P_0$  as the wetting phase pressure at  $z = 0$ . We denote the molar fraction of  $b$  dissolved in  $w$  with  $x_b$ . Taking the contribution of gravity into account, we can write the chemical potential of  $b$  dissolved in  $w$  at position  $z$  as  $m_b^w = m_b^0 + RT \ln \frac{x_b}{x_{b0}} - V_{mb} \Delta \rho g z$  (Muskat 1930, Sage and Lacey 1939), where  $m_b^0$  is the reference chemical potential of pure  $b$  at  $P_0$  and  $x_{b0}$  is the reference molar fraction of  $b$  dissolved in  $w$  at  $P_0$ . Similarly, the chemical potential of pure  $b$  within each bubble can be expressed as  $m_b = m_b^0 + V_{mb} (P_c - \Delta \rho g z)$ , where  $P_c$  is the capillary pressure at the bubble interface. For simplicity, we assume that  $x_b$  at  $z = 0$  and  $z = L_t$  is equal to the equilibrium concentration at the bubble surface at all times. We can therefore calculate it by equating  $m_b^w$  and  $m_b$  to obtain  $x_b|_{z=0, L_t} = x_{b0} \exp(\frac{V_{mb} P_c}{RT})$ . Finally, we initialize the dissolved  $\text{CO}_2$  concentration in the throat by uniformly setting it to  $x_b|_{t=0} = x_{b0} \exp(\frac{V_{mb} P_{c0}}{RT})$ , where  $P_{c0}$  is the initial bubble capillary pressure.

Having described the problem setup, we can now write the governing equations for the two-bubble system. The first equation is a species balance for the dissolved component  $b$  along the throat described by equation (1). Note that equation (1) is obtained by combining mass conservation with Fick's law for molecular diffusion. We have used the generalized Fick's law, which describes the dependence of molar mass flux  $J_b$  on chemical potential gradient, i.e.,

$$J_b = -\frac{Dc_b}{RT} \frac{\partial m_b^w}{\partial z}. \quad (1)$$

$D$  is the diffusion coefficient and  $c_b = x_b/V_{mw}$ . We can simplify the non-linear equation (1) by linearizing it around the reference pressure  $P_0$ . Specifically, we take  $P_0$  to be orders of magnitude larger than both  $P_{c0}$  and  $\Delta\rho gL_t$ . Under these conditions, quite typical in geologic CO<sub>2</sub> storage,  $x_{b/t=0}$  becomes orders of magnitude larger than any variations in  $x_b$ . We can therefore make the approximation outlined on the right-hand-side (RHS) of equation (1).

$$\frac{\partial x_b}{\partial t} = \frac{Dx_b}{RT} \frac{\partial^2 m_b^w}{\partial z^2} \approx D \frac{\partial^2 x_b}{\partial z^2} \quad (1)$$

The boundary conditions of equation (1) consist of setting  $x_b$  to the equilibrium  $x_b|_{z=0}$ ,  $L_t$  concentration derived above. To close the system, we need equations describing the evolution of the bubble volumes over time. This is achieved by simply imposing mass conservation at the interface between the bubble surface and the throat entrances. The result is equation (2) and (3).

$$\frac{dV_{bubble}}{dt} \Big|_{bottom} = \frac{A_t DV_{mb}}{RTV_{mw}} x_b \frac{\partial m_b^w}{\partial z} \Big|_{z=0} \quad (2)$$

$$\frac{dV_{bubble}}{dt} \Big|_{top} = -\frac{A_t DV_{mb}}{RTV_{mw}} x_b \frac{\partial m_b^w}{\partial z} \Big|_{z=L_t} \quad (3)$$

## 2.2. Results and Discussion

We solve equation (1)-(3) numerically with input parameters corresponding to typical CO<sub>2</sub>-water systems at ~1km depth (see Table S1) (Chiquet et al. 2007, Duan and Sun 2003, Lu

et al. 2013). Figs. 2(b-c) show the evolution of the two bubble volumes for different  $L_t$  and  $R_0$  (see Text S1). In all cases,  $\text{CO}_2$  is transferred from the bottom bubble to the top bubble. However, two different regimes can be identified. In *regime I*, the bottom bubble shrinks and the top bubble grows but they both stop at some finite equilibrium size. In *regime II*, the bottom bubble disappears completely and its mass is entirely transported into the top bubble. The occurrence of either regime is governed by the relative importance of capillary versus gravitational forces in this two-bubble system. Specifically, regimes I and II correspond to dominating capillary and gravitational forces, respectively. Increasing  $L_t$  (proportional to gravitational potential difference) and  $R_0$  (inversely proportional to capillary forces) can drive the system from regime I to II.

In order to better understand the regimes, we proceed to derive scaling relationships for each regime and verify them against numerical solutions of equation (1)-(3). We first simplify equation (1)-(3) by assuming that the rate of molecular diffusion along the throat is much faster than the rate of change in bubble volumes. Diffusion is therefore regarded as a quasi-static process limited by changes in bubble volumes. Under these conditions, the time derivative term in equation (1) can be neglected, and integration of equation (1) over  $z$  thus yields equation (4).

Note that equation (4) is simplified by approximating  $\frac{V_{mb} P_c}{RT} \ll \frac{V_{mb} (P_c + P)}{RT} \sim O(1)$ . Note that

$\Delta P_c$  is the capillary pressure difference between the two bubbles, which in turn depends on the bubble volumes. The latter is governed by equation (5), which we obtain by subtracting equation (2) from equation (3). Equation (5) is further simplified on the RHS by linearizing the chemical potential gradient (similar to section 2.1) and combining the result with equation (4).

Note that equation (5) suggests that, aside from  $L_t$ , the ripening process directly depends on  $A_t$ ,  $D$  and  $x_{b0}$ .

$$\frac{\partial x_b}{\partial z} = x_0 \left( \exp\left(\frac{V_{mb} P_c}{RT}\right) \Big|_{top} - \exp\left(\frac{V_{mb} P_c}{RT}\right) \Big|_{bottom} \right) \approx \frac{x_0 V_{mb}}{RT} DP_c \quad (4)$$

$$\frac{d(DV_{bubble})}{dt} = \left( \frac{A_t DV_{mb}}{RTV_{mw}} x_b \frac{\partial m_b^w}{\partial z} \right) \Big|_{bottom}^{top} \approx \left( 2A_t D \frac{V_{mb}}{V_{mw}} \frac{x_0 V_{mb}}{RT} \right) \left( \frac{DP_c - DrgL_t}{L_t} \right) \quad (5)$$

We now use equation (4) and (5) to derive scaling relations between the time required to reach equilibrium,  $t_e$ , and throat length,  $L_t$ . We define  $t_e$  as the time at which 99% of the cumulative mass transfer between the two bubbles is complete. In regime I, capillarity dominates and we can approximate  $P_c \approx \gamma m_2 V_{bubble}$ . Subsequent integration of equation (5) yields equation (6). Invoking our definition for  $t_e$  we obtain  $\Delta P_c / \Delta \rho g L_t = 0.99$ , which upon

substituting it into equation (6) yields  $\ln 0.01 = -2A_t D \frac{V_{mb}}{V_{mw}} \frac{x_0 V_{mb}}{RT} g m_2 \frac{t_e}{L_t}$ . We thus obtain a

linear  $t_e \sim L_t$  scaling for regime I, which is different from  $t_e \sim L_t^2$  in classical Fickian diffusion (Whitaker 1967). In regime II, since gravity dominates, we can neglect the capillary term in equation (5) and integrate to yield equation (7). We thus see that  $t_e$  is independent of  $L_t$  in regime II. As an aside, notice that  $t_e$  depends on  $\gamma$  only in regime I and on  $\Delta \rho$  only in regime II.

$$\ln \left( 1 - \frac{\Delta P_c}{\Delta r g L_t} \right) = -2A_t D \frac{V_{mb}}{V_{mw}} \frac{x_0 V_{mb}}{RT} \frac{g m_2}{L_t} t \quad (6)$$

$$t_e = V_0 / \left( A_t D \frac{V_{mb}}{V_{mw}} \frac{x_0 V_{mb}}{RT} \Delta r g \right) \quad (7)$$

We test the validity of the above scaling relations between  $t_e$  and  $L_t$  by plotting numerical simulation data in an alternative dimensionless form. Namely, we plot the dimensionless equilibrium time  $t_d = m_2 A_t D t_e$  against the dimensionless throat length

$L_d = \frac{V_{mw}}{V_{mb}} \frac{RT}{x_0 V_{mb} g} L_t$  in Fig. 2(d). As expected, all data points in regime I collapse onto a single

straight line and all the data points in regime II plateau into constant values. The peaks in Fig.

2(d) correspond to a regime, in which capillary and gravity forces are comparable in magnitude. In this case,  $P_c \approx \gamma m_2 V_{bubble}$  is not a good approximation and accurate predictions require computation.

As a sidelight, we note that ripening happens majorly among neighboring pores. Therefore  $L_t$  is much smaller than 1mm thus evolution of two neighboring identical bubbles always fall in regime I in most cases. However, much larger  $L_t$  (up to centimeters) may be realistic when describing ripening between gas ganglia trapped in neighboring micro-fractures or vugs (i.e. with large  $R_0$  thus smaller  $m_2$ ), in which case the evolution dynamics may fall into regime II.

### 3. Upscaling from Pore Scale to Continuum Scale

The above pore-scale analysis demonstrated that gravity-induced ripening causes bubbles at the shallower depths to grow at the expense of bubbles at deeper strata. To understand the implications of this observation over geologic scales (meters in thickness and thousands of years), we develop a simplified one-dimensional continuum model based on the pore-scale results of section 2. We recognize that geologic CO<sub>2</sub> storage is a multiscale multiphysics problem that does not easily lend itself to simplifications. However, reduced-order models are very valuable in that they allow the effects of a subset of the physics to be rapidly analyzed and extrapolated over engineering scales for the purposes of project design and operations. Our aim here is to achieve exactly such an understanding of the long-term effects of gravity-induced Ostwald ripening.

For realistic geological systems,  $L_t$  is always sufficiently small for the quasi-static assumption leading to equation (5) to be valid. Equation (5) is also consistent with a previously validated model for bubble ripening (excluding gravity) at the scale of multiple interconnected

pores (Xu et al. 2017). We proceed by defining a modified Henry's constant as  $K^{px} = \partial P_b / \partial x_b$ ; similar to (Xu et al. 2017). We also define the average number of bubbles residing in adjacent pores of a trapped bubble as  $n$ . Adjacency means that there is a throat connecting the two bubbles. We can now impose mass conservation on each bubble via equation (8).

$$\frac{dV_{bubble}}{dt} = kn \frac{\overline{DP_b}}{L_t}, \quad \text{where } k \approx \frac{V_{mb} A_t D}{V_{mw} K^{px}}$$

(8)

In equation (8),  $\overline{DP_b}$  is the average potential difference between a bubble and its neighboring bubbles. The total potential of each bubble is  $P_b = P_c - \Delta \rho g z + P_0$ . Equation (8) is a generalization of a previously reported model (Xu et al. 2017) that accounts for gravity. Notice that equation (8) has a discrete form as it applies between individual bubbles. In order to transform equation (8) into a differential or continuum form, we can first take its limit as  $L_t \rightarrow 0$ , and assume that all pores are identical, to obtain equation (9) (details in Supplementary materials).

$$\frac{\partial (V_{bubble} / V_{pore})}{\partial t} = \left( \frac{kn_0 L_{pore}^2}{V_{pore} 2L_t} \right) \cdot \frac{\partial}{\partial z} \left( \frac{n}{n_0} \frac{\partial P_b}{\partial z} \right)$$

(9)

In equation (9),  $L_{pore}$  is the center-to-center distance between two neighboring pores and  $V_{pore}$  is the volume of each pore.  $n_0$  is the number of neighboring pores (not bubbles) adjacent to each pore. Here we introduce an assumption of local capillary equilibrium, i.e., bubbles in an REV (representative elementary volume) are in equilibrium, sharing identical capillary pressure as well as gravitational potential. That said, although there could be complex interactions among multiple neighboring bubbles, the time required to get equilibrium inside an REV (< cm) is negligible compared to that of gravity-driven ripening process. Therefore,

we ignore the complex dynamics in an REV and always assume local thermodynamic equilibrium, similar to most of other large-scale simulations.

Further, if we denote  $V_{bubble}/V_{pore}$  as the non-wetting phase saturation  $S$  and  $n/n_0$  as the “pore occupancy” parameter  $C$  (i.e., fraction of neighboring pores occupied by bubbles), equation (9) is rewritten into the one-dimensional continuum model given by equation (10). Note that we have implicitly assumed uniformity of all dependent and independent variables across any given depth  $z$ .

$$\frac{dS}{dt} = K \frac{d}{dz} \left( C \frac{dP_b}{dz} \right), \quad \text{where } P_b = P_c - \Delta \rho g z + P_0 \quad (10)$$

Both  $P_c$  and  $C$  are functions of  $S$  (detailed in Supplementary Material). The rate constant is

given by  $K = n_0 B_0 F_0$ , where  $B_0 = \frac{A_t}{V_{pore}} \frac{L_{pore}^2}{2L_t}$  depends only on pore shape (not size) and

$F_0 = \frac{V_{mb}}{V_{mw}} \frac{D}{K^{px}}$  depends only of fluid properties. Without loss of generality, we assume  $B_0 = 1$ .

$P_c$  is the local capillary pressure of trapped bubbles, which is different from the conventional definition of capillary pressure in typical continuum (or Darcy) models. The latter corresponds to a continuous non-wetting phase relevant in fluid-fluid displacement process (Andrew, Bijeljic and Blunt 2014).

## 4. Continuum Scale Simulation Results and Discussion

### 4.1. A Demonstration Case

We solve equation (10) numerically to predict the long-term evolution of gravity-induced Ostwald ripening after supercritical CO<sub>2</sub> injection into a 1 m thick stratum. We set  $C = 1$  at the beginning of the simulation. The profile of CO<sub>2</sub> saturation versus depth is randomly

initialized from a uniform distribution with mean residual saturation  $S_r = 0.3$ . We use CO<sub>2</sub> and water properties corresponding to 10 MPa and 60 °C typical of ~1 km depths (see Table S1) (Chiquet et al. 2007, Duan and Sun 2003, Lu et al. 2013).

Fig. 3(a)-(d) shows that within a geologically short time after injection (~1 year), the saturation profile becomes locally uniform. This observation agrees with previous experimental studies in the absence of gravity (Garing et al. 2017, Xu et al. 2017). Several decades (~60 years) later, the onset of vertical redistribution of CO<sub>2</sub> emerges. During this time, CO<sub>2</sub> is transferred from deeper strata towards shallower depths leaving a bubble-free zone at the bottom. When the CO<sub>2</sub> saturation at the top of the reservoir reaches a critical value ( $S_{max} = 0.7$  in this case study), bubbles coalesce into a continuous mobile gas cap. Finally, 2000 years after injection, the CO<sub>2</sub> saturation profile reaches an equilibrium configuration, in which capillary trapping dominates only in an interval between the gas cap and the bubble-free zone. We refer this interval as the “stable capillary trapping belt” (SCTB). This case study shows that even though 100% of the initially trapped CO<sub>2</sub> is in the form of isolated bubbles, a mobile gas cap is eventually formed at the top of the formation (i.e.,  $S > S_{max}$ ).

It is noteworthy that the gas cap forms far earlier than mineral trapping can have any significant impact on either the injected CO<sub>2</sub> or the rock matrix (Gasda et al. 2011, Krevor et al. 2015, Xu et al. 2004) in this case study. While ~ 1 m thick strata are quite typical as hydrocarbon reservoirs or shallow water aquifers, they are likely too thin to be considered ideal storage sites. In the next section, we develop dimensional analysis on ripening dynamics based on equation (10), and study the scaling of gas cap growth as well as equilibrium time with more simulation results. Therefore, we extend our discussion to thicker stratum over longer time scales.

#### 4.2. Scaling of Ripening Dynamics and Equilibrium

Assuming that capillarity is only locally significant, dimensional analysis of equation (10) yields the scaling between time  $\Delta t$  and the corresponding change in gas cap thickness  $\Delta L$ :

$$\frac{S_r}{Dt} \sim K \frac{DP_b}{DL^2} = K \frac{Dr_g}{DL} \quad (11)$$

Denoting the gas cap thickness by  $h_c$ , and assuming  $h \gg h_c$ , equation (11) can be transformed into equations (12) for estimating the growth of a gas cap:

$$h_c \sim \frac{Dr_g K}{S_r} t \quad (12)$$

Note that  $h_c$  is proportional to  $t$ , instead of  $t^{1/2}$ , and does not depend on  $h$ . Equation (12) agrees with the numerical simulations in Fig. 3(e) during the growth stage of the gas cap. If the formation is sufficiently thick, a  $\sim 3$  m thick gas cap may form after 10,000 years. Equation (11) can also be transformed to estimate the time needed to reach equilibrium  $t_{eq}$ :

$$t_{eq} \sim \frac{S_r}{Dr_g K} h \quad (13)$$

With a factor 0.6 multiplying the RHS, equation (13) agrees well with numerically simulated  $t_{eq}$  for  $h$  between 1m and 100 m as shown in Fig. 3(f). We see that it takes  $\sim 8000$  years for a 5 m thick stratum and  $\sim 80000$  years for a 50 m thick stratum to reach equilibrium. For such thick strata, the time scale of gravity-driven ripening is comparable to that of mineral trapping, which complicates the accurate prediction of the fate of stored CO<sub>2</sub>.

The final shape of the macroscopic saturation profile depends on the competition between gravity and capillary forces in the reservoir. In the Supplementary Material (section S2.5), we show that the SCTB thickness,  $h_{SCTB}$ , can be calculated by solving  $\max[P_c(S)] - \min[P_c(S)] = \Delta\rho g h_{SCTB}$ . If capillarity dominates,  $h_{SCTB}/h \gg 1$  and capillary trapping is globally stable (similar to regime I at the pore scale). If gravity dominates,  $h_{SCTB}/h \ll 1$  and almost all

of the trapped CO<sub>2</sub> evolves into an overlying gas cap (similar to regime II at the pore scale). This is confirmed by Fig. 3(g)-(i).

Equations (12) and (13) may be applied to devise strategies to decelerate gravity-induced ripening for reducing the risk of gas-cap formation and leakage. In practice, they

involve either decreasing  $K$  or  $\Delta\rho$ ; recall  $K=n_0B_0F_0$  where  $B_0 = \frac{A_t}{V_{proe}} \frac{L_{pore}^2}{2L_t}$  and  $F_0 = \frac{V_{mb}}{V_{mw}} \frac{D}{K^{px}}$ ,

which are very sensitive to the thermodynamic properties of CO<sub>2</sub>. Therefore, storage sites with low temperature, high pressure, and high salinity are preferred scenarios, which seem representative of strata underneath deep seafloors. On the other hand, drilling and injection into deep offshore strata is both economically expensive and ecologically risky (Eccles et al. 2009), which must be taken into assessment.

#### 4.3. Limits of the Proposed Models

The analysis in this paper focused on a single geological stratum. For intervals consisting of multiple strata, equation (10) remains valid in each storage layer except in the cap rock. One reason for this is that cap rocks consist of very small pores and thus very high capillary entrance pressures that injection pressures cannot overcome. This violates assumptions (5) and (7) listed in the Supplementary Material (section S.3). Classical single-phase Fickian diffusion may be more appropriate for describing CO<sub>2</sub> migration within cap rocks, although the exact physics are debated (Neuzil and Person 2017, Neuzil 2013). A detailed study is deferred to the future.

Throughout this work, we also neglected the impact of CO<sub>2</sub> dissolution on brine density. It is known that CO<sub>2</sub> dissolution increases brine density, which in turn induces Rayleigh-Taylor instabilities and convective dissolution (Thomas, Dehaeck and De Wit 2018, Neufeld et al. 2010, Loodts et al. 2014). While not captured by our model, we argue that convective

dissolution and gravity-induced ripening occur at different stages of the CO<sub>2</sub> sequestration process. Convective dissolution typically occurs at the underside edges of an overriding CO<sub>2</sub> plume and is driven by density differences within the brine phase. By contrast, gravity-induced ripening is driven by density differences between two un-dissolved phases. Our models assume that the surrounding brine is already saturated with dissolved CO<sub>2</sub>, which is representative of the region adjacent to the wellbore in the wake of an injected CO<sub>2</sub> plume. Incidentally, the same region will have undergone an initial drainage (by CO<sub>2</sub>) followed by a subsequent imbibition (by brine) leading to trapped CO<sub>2</sub> bubbles and ganglia. The brine in this region is likely to have had sufficient time to be saturated by CO<sub>2</sub>, rendering density differences within the brine of secondary importance. Nevertheless, future work must confirm this hypothesis by including convection in the modeling framework.

We note that gravity-induced ripening may also play a crucial role in geologic fluid emplacement and migration (e.g., hydrocarbons). The millions of years in time scale match our model predictions for thick strata. That said, the model must be generalized to include multi-component geochemistry and mixed-wettability, if it is to correctly capture hydrocarbon migration.

## **5. Conclusions**

We develop pore-scale and continuum models of gravity-induced Ostwald ripening. The models demonstrate that capillary trapping may not be as stable a trapping mechanism as previously assumed. We show that gravity can induce the redistribution of otherwise hydrodynamically stable bubbles and transport significant quantities of CO<sub>2</sub> from deeper strata towards shallower depths over geologic time scales. The result may be the formation of a gas cap at the top of the reservoir. The time scale of this process is predicted to be less than or

comparable to that of mineral trapping. We outline potential strategies for decelerating the ripening rate by a careful selection of CO<sub>2</sub> storage sites. The above findings, while subject to several assumptions, may provide new insights for assessing CO<sub>2</sub> storage security. The findings herein might also be of relevance to gravity-induced ripening in the context geologic fluid emplacement and migration over millions of years (e.g., hydrocarbons).

**Acknowledgements:** Authors declare no competing interests. All parameters used are available in the main text or in the Supporting Information texts with necessary references. We aim at establishing a zero-order conceptual model thus no field data is applied.

#### **References:**

- Andrew, M., B. Bijeljic & M. J. Blunt (2014) Pore-by-pore capillary pressure measurements using X-ray microtomography at reservoir conditions: Curvature, snap-off, and remobilization of residual CO<sub>2</sub>. *Water Resources Research*, 50, 8760-8774.
- Benson, S. M., K. Bennaceur, P. Cook, J. Davison, H. de Coninck, K. Farhat, C. Ramirez, D. Simbeck, T. Surlis & P. Verma (2012) Carbon capture and storage. *Global energy assessment-Toward a sustainable future*, 993.
- Benson, S. M. & D. R. Cole (2008) CO<sub>2</sub> sequestration in deep sedimentary formations. *Elements*, 4, 325-331.
- Benson, S. M. & F. M. Orr (2008) Carbon dioxide capture and storage. *MRS bulletin*, 33, 303-305.
- Chiquet, P., J.-L. Daridon, D. Broseta & S. Thibeau (2007) CO<sub>2</sub>/water interfacial tensions under pressure and temperature conditions of CO<sub>2</sub> geological storage. *Energy Conversion and Management*, 48, 736-744.
- de Chalendar, J. A., C. Garing & S. M. Benson (2018) Pore-scale modelling of Ostwald ripening. *Journal of Fluid Mechanics*, 835, 363-392.
- Duan, Z. & R. Sun (2003) An improved model calculating CO<sub>2</sub> solubility in pure water and aqueous NaCl solutions from 273 to 533 K and from 0 to 2000 bar. *Chemical geology*, 193, 257-271.
- Eccles, J. K., L. Pratson, R. G. Newell & R. B. Jackson (2009) Physical and economic potential of geological CO<sub>2</sub> storage in saline aquifers. *Environmental science & technology*, 43, 1962-1969.
- Fu, X., L. Cueto-Felgueroso & R. Juanes (2016) Thermodynamic coarsening arrested by viscous fingering in partially miscible binary mixtures. *Physical Review E*, 94, 033111.
- Garing, C., J. A. de Chalendar, M. Voltolini, J. B. Ajo-Franklin & S. M. Benson (2017) Pore-scale capillary pressure analysis using multi-scale X-ray micromotography. *Advances in Water Resources*, 104, 223-241.
- Gasda, S., J. Nordbotten & M. Celia (2011) Vertically averaged approaches for CO<sub>2</sub> migration with solubility trapping. *Water Resources Research*, 47.

- Gasda, S. E., J. M. Nordbotten & M. A. Celia (2009) Vertical equilibrium with sub-scale analytical methods for geological CO<sub>2</sub> sequestration. *Computational Geosciences*, 13, 469.
- Guo, B., K. W. Bandilla, F. Doster, E. Keilegavlen & M. A. Celia (2014) A vertically integrated model with vertical dynamics for CO<sub>2</sub> storage. *Water Resources Research*, 50, 6269-6284.
- Hagoort, J. 1988. *Fundamentals of gas reservoir engineering*. Elsevier.
- Hesse, M. A., F. M. Orr & H. Tchelepi (2008) Gravity currents with residual trapping. *Journal of Fluid Mechanics*, 611, 35-60.
- Huppert, H. E. & J. A. Neufeld (2014) The fluid mechanics of carbon dioxide sequestration. *Annual Review of Fluid Mechanics*, 46, 255-272.
- Ide, S. T., K. Jessen & F. M. Orr Jr (2007) Storage of CO<sub>2</sub> in saline aquifers: Effects of gravity, viscous, and capillary forces on amount and timing of trapping. *International Journal of Greenhouse Gas Control*, 1, 481-491.
- Juanes, R., E. Spiteri, F. Orr & M. Blunt (2006) Impact of relative permeability hysteresis on geological CO<sub>2</sub> storage. *Water resources research*, 42.
- Krevor, S., M. J. Blunt, S. M. Benson, C. H. Pentland, C. Reynolds, A. Al-Menhali & B. Niu (2015) Capillary trapping for geologic carbon dioxide storage—From pore scale physics to field scale implications. *International Journal of Greenhouse Gas Control*, 40, 221-237.
- Loodts, V., C. Thomas, L. Rongy & A. De Wit (2014) Control of convective dissolution by chemical reactions: General classification and application to CO<sub>2</sub> dissolution in reactive aqueous solutions. *Physical review letters*, 113, 114501.
- Lu, W., H. Guo, I.-M. Chou, R. Burruss & L. Li (2013) Determination of diffusion coefficients of carbon dioxide in water between 268 and 473 K in a high-pressure capillary optical cell with in situ Raman spectroscopic measurements. *Geochimica et Cosmochimica Acta*, 115, 183-204.
- Muskat, M. (1930) Distribution of non-reacting fluids in the gravitational field. *Physical Review*, 35, 1384.
- Neufeld, J. A., M. A. Hesse, A. Riaz, M. A. Hallworth, H. A. Tchelepi & H. E. Huppert (2010) Convective dissolution of carbon dioxide in saline aquifers. *Geophysical research letters*, 37.
- Neuzil, C. (2013) Can shale safely host US nuclear waste? *Eos, Transactions American Geophysical Union*, 94, 261-262.
- Neuzil, C. E. & M. Person (2017) Reexamining ultrafiltration and solute transport in groundwater. *Water Resources Research*, 53, 4922-4941.
- Pentland, C. H., R. El-Maghraby, S. Iglauer & M. J. Blunt (2011) Measurements of the capillary trapping of super-critical carbon dioxide in Berea sandstone. *Geophysical Research Letters*, 38.
- Perkins, T. & O. Johnston (1963) A review of diffusion and dispersion in porous media. *Society of Petroleum Engineers Journal*, 3, 70-84.
- Sage, B. H. & W. N. Lacey (1939) Gravitational concentration gradients in static columns of hydrocarbon fluids. *Trans. AIME*, 132, 120-131.
- Thomas, C., S. Dehaeck & A. De Wit (2018) Convective dissolution of CO<sub>2</sub> in water and salt solutions. *International Journal of Greenhouse Gas Control*, 72, 105-116.
- Thompson, K. E. (2002) Pore-scale modeling of fluid transport in disordered fibrous materials. *AIChE Journal*, 48, 1369-1389.
- Voorhees, P. W. (1985) The theory of Ostwald ripening. *Journal of Statistical Physics*, 38, 231-252.

Voorhees, P. W. (1992) Ostwald ripening of two-phase mixtures. *Annual Review of Materials Science*, 22, 197-215.

Whitaker, S. (1967) Diffusion and dispersion in porous media. *AIChE Journal*, 13, 420-427.

Xu, K., R. Bonnecaze & M. Balhoff (2017) Egalitarianism among Bubbles in Porous Media: An Ostwald Ripening Derived Anticoarsening Phenomenon. *Physical review letters*, 119, 264502.

Xu, T., J. A. Apps & K. Pruess (2004) Numerical simulation of CO<sub>2</sub> disposal by mineral trapping in deep aquifers. *Applied geochemistry*, 19, 917-936.

Accepted Article

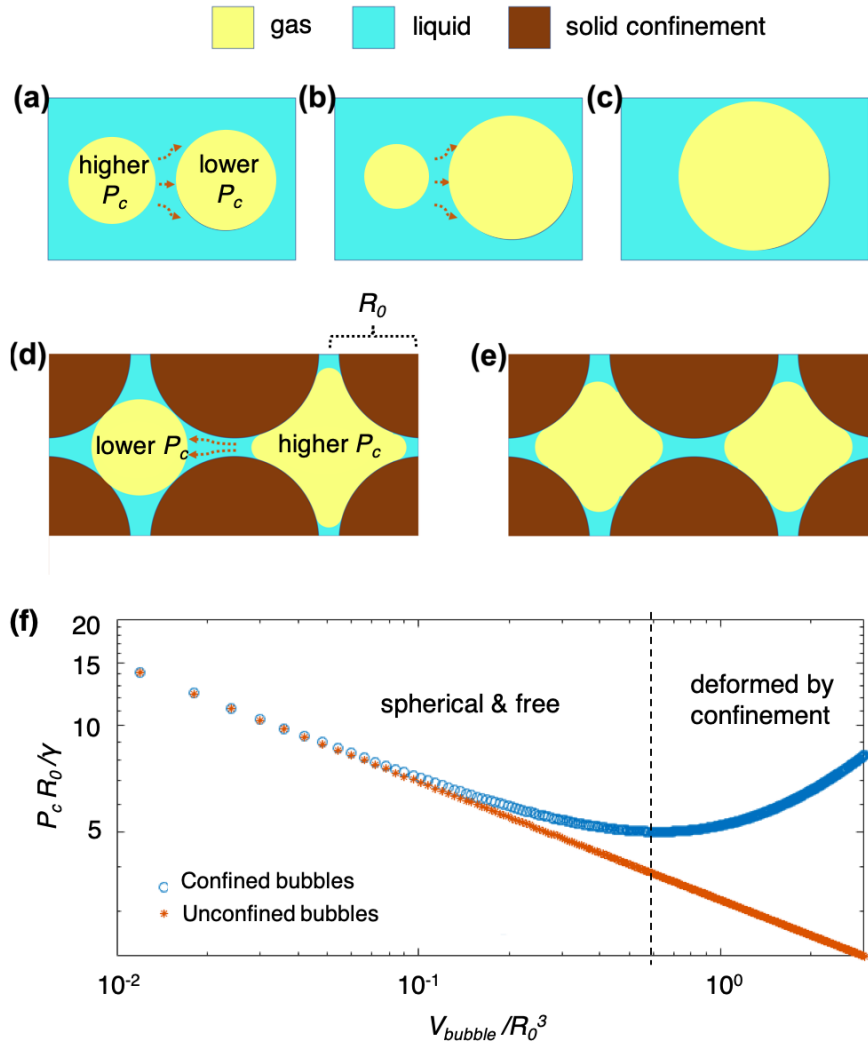


**Figure 1.** Ostwald ripening in the presence and absence of confinement, without gravity. (a)-(c) In unconfined space, ripening leads to bubble coarsening. (d)-(e) In confined pores (here identically shaped), ripening results in stable bubbles with identical curvature.  $R_0$  is the distance between the pore center to the throat center. (f) Dimensionless capillary pressure versus dimensionless bubble volume for a bubble in the presence (blue) and absence (red) of confinement. The dashed line represents  $V_{crit}$  at  $P_{c,min}$ .

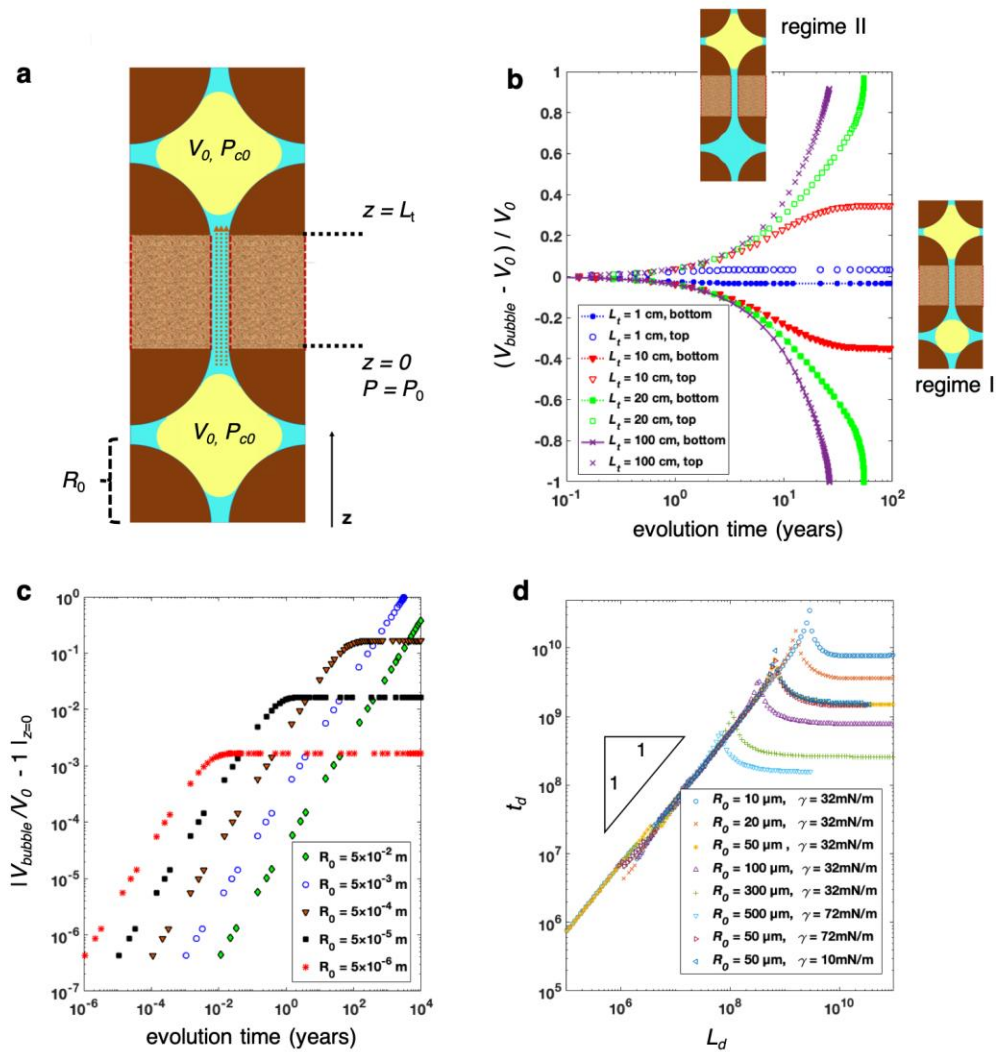


**Figure 2.** Simplified pore-scale model of gravity-induced ripening for a two-bubble system. (a) Schematic of the system setup at  $t = 0$ .  $L_t$  and  $R_0$  are not to scale. Evolution of the (normalized) bubble volumes over time at (b) fixed  $R_0 = 50 \mu\text{m}$  with varying  $L_t$ , and at (c) fixed  $L_t = 5 \text{ mm}$  with varying  $R_0$ . Note that there are two equilibrium regimes. Regime I at small  $L_t$  and  $R_0$ , and regime II at large  $L_t$  and  $R_0$ . (d) Plot of dimensionless equilibrium time ( $t_d$ ) versus dimensionless throat length ( $L_d$ ). Note that we don't show the results for  $L_t \ll 1 \text{ cm}$  in (b) as they all fall into regime I, although those data have been incorporated in (d).

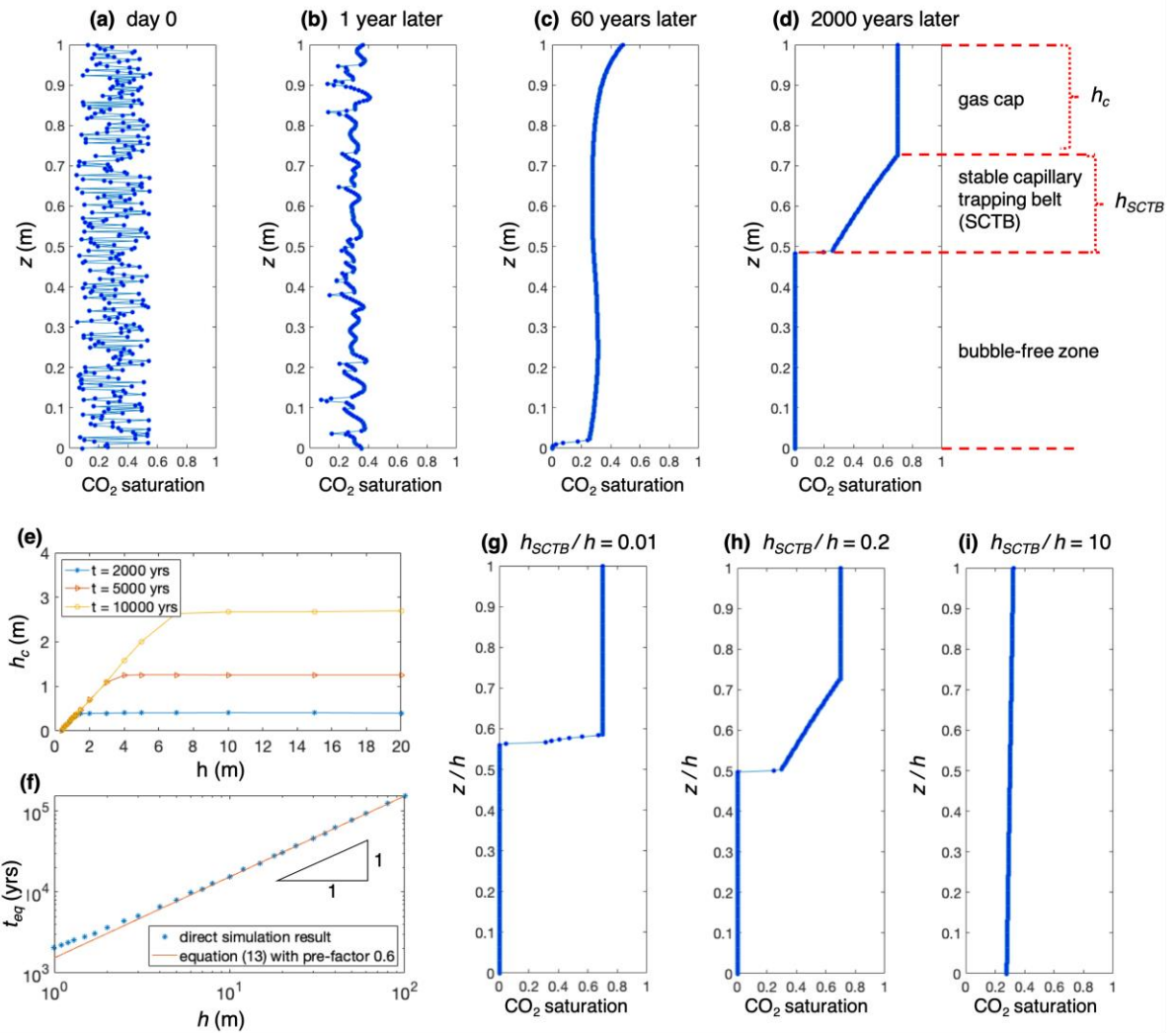


**Figure 3.** Top row: evolution of the vertical CO<sub>2</sub> saturation profile in a 1 m thick stratum at 10 MPa and 60 °C, corresponding to Movie S1. (a) Initially randomly distributed saturation profile; (b) one year after injection, capillary forces dominate and the profile becomes locally uniform; (c) 60 years later, gravity dominates and the onset of vertical CO<sub>2</sub> migration is seen; (d) 2000 years later, ripening is complete and the saturation profile consists of three regions: a mobile gas cap at the top, a stable capillary trapping zone, and a bubble-free zone at the bottom. Bottom row: (e) gas cap thickness,  $h_c$ , as a function of formation thickness,  $h$ , and time; (f) time required to reach equilibrium,  $t_{eq}$ , for different  $h$ . Similar thermodynamic and pore-scale parameters are used in (a)-(f). (g)-(i) Equilibrium CO<sub>2</sub> saturation profiles with  $S_r = 0.3$  for  $h_{SCTB}/h = 0.01, 0.2, \text{ and } 10$ .